

# FAINT, MOVING OBJECTS IN THE HUBBLE DEEP FIELD: COMPONENTS OF THE DARK HALO?<sup>1</sup>

RODRIGO A. IBATA<sup>2</sup>, HARVEY B. RICHER<sup>3</sup>, RONALD L. GILLILAND<sup>4</sup> & DOUGLAS SCOTT<sup>3</sup>

*Submitted to The Astrophysical Journal Letters*

## ABSTRACT

The deepest optical image of the sky, the Hubble Deep Field (HDF), obtained with the Hubble Space Telescope (HST) in December 1995, has been compared to a similar image taken in December 1997. Two very faint, blue, isolated and unresolved objects are found to display a substantial apparent proper motion,  $23 \pm 5$  mas/yr and  $26 \pm 5$  mas/yr; a further three objects at the detection limit of the second epoch observations may also be moving. Galactic structure models predict a general absence of stars in the color-magnitude range in which these objects are found. However, these observations are consistent with recently-developed models of old white dwarfs with hydrogen atmospheres, whose color, contrary to previous expectations, has been shown to be blue. If these apparently moving objects are indeed old white dwarfs with hydrogen atmospheres and masses near  $0.5 M_{\odot}$ , they have ages of approximately 12 Gyr, and a local mass density that is sufficient, within the large uncertainties arising from the small size of the sample, to account for the entire missing Galactic dynamical mass.

*Subject headings:* Galaxy: halo – solar neighbourhood – dark matter – stars: white dwarfs

## 1. INTRODUCTION

The MACHO collaboration have found  $\sim 16$  massive compact halo objects (MACHOs) in their 4 year survey for microlensing towards the Large Magellanic Cloud (Alcock *et al.* 1997). Based on the standard multiple component mass model for the Galaxy (Griest 1991), they conclude that this lensing rate is much higher than the Galactic thick disk and Galactic stellar halo can account for, and argue that the lenses are stellar-mass objects that reside in an extended halo around the Galaxy and constitute a sizeable fraction, perhaps half, of its mass. This population should also be present in the Solar neighborhood, and in principle could be seen in deep or wide field surveys, if the individual components are sufficiently luminous.

We set out to investigate whether the HDF (Williams *et al.* 1995; hereafter W95) could be used, in conjunction with images in the same field taken two years later, to measure proper motions (PMs) of faint stars that could be nearby MACHO candidates. Though the HDF covers a small area,  $0.0015^{\circ}$ , it is very deep (reaching to  $V \sim 28$ ), so the volume probed for faint Galactic sources is considerable. Earlier starcount studies in the HDF (Flynn *et al.* 1996; Elson *et al.* 1996; Méndez *et al.* 1996) were not able to reach to the faint limit of the dataset due to star-galaxy confusion at magnitudes fainter than  $V = 26.5$ . PMs provide a means to perform further star-galaxy discrimination, since anything with significant PM cannot be very distant.

## 2. REGISTRATION OF THE HUBBLE DEEP FIELD FRAMES

Our second epoch HDF exposures, obtained in December 1997 in the same field as the original HDF, give a baseline of almost exactly two years and have total integration of 27.3 Ksec in U (F300W) and 63 Ksec in I (F814W).

These exposures were obtained at several slightly offset positions, and at approximately the same orientation as the originals. For the present work, we used only the I-band data to determine PMs.

The PMs of stars are measured as an angular displacement between epochs with respect to some reference frame; the accuracy of this frame is therefore one of the crucial limiting factors affecting the accuracy of the PM measurements. The determination of an accurate reference frame is not entirely straightforward due to the optical distortions of the cameras and irregularities in the construction of the detectors. Fortunately, these instrumental signatures are stable, and so their effects can be largely eliminated. The approach we took for constructing the reference frame in each field was to obtain differential measurements of the positions of  $\sim 50$  bright, compact galaxies on each frame, and, by adopting a model for the optical distortion of the WFPC2 mosaic (Trauger *et al.* 1995), determine a simple linear transformation relating the distortion-corrected frames. The accuracy of this registration is better than 2 milli-arcseconds (mas), judging from the rms scatter in the positions of the reference galaxies. In order to obtain an independent check of the registration precision, we created a set of new frames by resampling the original data onto the same grid as the reference image adopted by W95, using the optical distortion model and the computed offsets. Cross-correlation of the images of both epochs against the reference image showed them to be aligned to an accuracy of better than 3 mas.

## 3. PROPER MOTION MEASUREMENTS

A maximum likelihood image center finding algorithm was developed for this project (Ibata & Lewis 1998). The important advantage of this technique is that it does not

<sup>1</sup>Based on observations with the NASA/ESA Hubble Space Telescope

<sup>2</sup>European Southern Observatory Karl Schwarzschild Straße 2, D-85748 Garching bei München, Germany

<sup>3</sup>Department of Physics & Astronomy, University of British Columbia, 2219 Main Mall, Vancouver, B.C., V6T 1Z4, Canada.

<sup>4</sup>Space Telescope Science Institute, 3700 San Martin Drive, Baltimore, MD 21218 USA.

use a combined frame for calculating the image centroids (avoiding the inevitable degradation of information) or a resolution-enhanced combined frame (which avoids also having correlated noise). By applying this technique to the HDF data, they showed that centroiding ( $1\sigma$ ) accuracies of  $\sim 10$  mas can be obtained for stars of magnitude  $I \sim 28$ , degrading to  $\sim 1$  mas for  $I < 25$ .

An input list of 443 compact objects (detected with DAOPHOT, Stetson 1987), was provided to the PM algorithm. In addition to finding the maximum-likelihood image centroids, the routine returns both the likelihood surface and  $P(R < 2.5)$ , the probability that the image data (within a radius of 2.5 pixels from the most likely centroid position) is drawn from the same distribution as the PSF. Objects for which  $P(R < 2.5) < 0.01$ , were considered to be extended and therefore discarded.

In this way, we detected 58 isolated point-sources, of which 40 have  $V > 27$ . The brighter ( $V < 27$ ) moving sources can be accounted for by known Galactic stellar populations. The calibrated  $V$ ,  $(V - I)$  color-magnitude diagram (on the AB system) of the faint subset is shown in Figure 1. The PM vectors are also plotted, either as black or green arrows. The axes have been chosen such that motion in the direction of Galactic longitude is parallel to the  $(V - I)$  color axis, whereas motion in the direction of Galactic latitude is parallel to the magnitude axis (increasing downwards). The PM scale on this plot is such that one abscissa or ordinate unit represents a motion of 100 mas (approximately one pixel on the Wide Field chips) over the two year baseline of the experiment. The red arrows are of length equal to the PM uncertainty in the direction of the PM.

Among the population of 40 faint point sources with  $V > 27$ , five are observed to have PMs that exceed the measurement uncertainty by more than a factor of 3. These objects are listed in Table 1. On the top row of Figure 2 we display co-added images,  $4''$  on a side, of the field around each of these objects; the middle two rows are high-resolution images which clearly show the centroid shifts between epochs; the bottom row shows the centroid likelihood contours given the data at each epoch.

#### 4. CHECKS OF THE CENTROID SHIFTS

Simulations were carried out to constrain the incompleteness of the observed sample and to check the PM uncertainties. In each simulation, we added 100 fake stars, of zero PM, into all the individual  $V$  and  $I$ -band frames. The stars were added uniformly between  $I = 25$  and  $I = 31$ , with a color of  $V - I = 0$ . As before, we calibrated the photometry, and rejected those objects for which  $P(R < 2.5) < 0.01$ , those that had photometric uncertainties  $\delta(V) > 0.5$ ,  $\delta(I) > 0.5$ , and those with a neighbor less than 1 arcsec away. Twenty such simulations were performed on each of the Wide Field chips for a total of 6000 artificial stars. The completeness of our sample at magnitudes between  $I = 27$  and  $I = 28$  is  $42\% \pm 2\%$ . It was found that the maximum deviation between epochs in the computed centroids of the artificial stars was 18 mas/yr, with the biggest deviation being 3.6 times its estimated uncertainty. The PMs of our five objects exceed even these maximum random values, indicating that the measured displacements are unlikely to occur by chance.

But what about systematic effects on our PM measure-

ments? There are several possible mechanisms which could have given rise to a false PM detection. The most obvious are cosmic rays, hot pixels, the inevitable Poisson noise, and construction irregularities of the detectors. The artificial star tests provide a convenient way to test these concerns. The simulated stars were placed into the individual data frames at exactly the same location at both epochs, so if by chance that location corresponds to a position where an unmasked contaminant remains, a false PM could be detected. We find that there is less than a 0.1% chance for displacements of the magnitude of those detected in the five faint objects listed in Table 1, so it is highly unlikely that the measured PMs have been affected in this way.

Nevertheless, we ran a further check to make sure that the PM measurements of the five apparently moving objects are not influenced by large noise spikes or defective pixels. In each test, we rejected all the data at one spacecraft pointing (i.e., ‘dither’), and re-computed the maximum-likelihood centroids. If there was a residual unmasked cosmic ray or a hot pixel, or even a particularly high Poisson deviation that was causing an incorrect PM measurement, the contaminant would be absent in one of the test runs, and so we would find a PM much closer to zero in that test run. However, the tests did not reveal such an effect, confirming that our results are not an artifact of residual cosmic rays, hot pixels or Poisson noise.

To check the five apparently high PM detections, we have implemented three other, more direct, techniques that operate on combined images; the results of these tests are listed in Table 1. We find that the PM measurements of objects 4–551, 2–766, and 4–492 are reproduced, within the uncertainties, by all four techniques. However, the PMs of 4–141 and 2–455 measured with the maximum-likelihood method are not verified by the other methods. For this reason we do not consider the PM measurements of the faint objects 4–141 and 2–455 to be secure. Nevertheless, we include all 5 objects in our discussion, since they represent the full sample of candidates discovered in our systematic survey for PMs in the HDF.

#### 5. THE NATURE OF THE FAINT, APPARENTLY MOVING, SOURCES

A natural explanation for the apparent large PMs of the five objects is that they could be detections of supernova (SN) events in high redshift star-forming galaxies. If the SNe were somewhat off-centered from their host galaxy, this would skew the light distribution at one epoch, causing a shift in the computed image centroid that is not due to actual PM. Indeed there is weak evidence that object 2–766 became fainter, by  $25\% \pm 13\%$  between the two epochs, which could be explained within this paradigm as being due to a SN in the first epoch dataset. However, there was no significant brightness variation in objects 4–551, 4–141, 4–492 and 2–455, implying that if there were SNe present in one of the epochs in each of these three hypothetical galaxies, they must have been extremely faint. Nevertheless, we should ask: is it possible that the computed maximum-likelihood object centroids could have been so substantially affected by such faint SNe to have given rise to the observed large apparent positional shift?

To answer this we conducted additional artificial star tests, adding point sources within  $0''.2$  of the moving candi-

dates to simulate the effect of SNe on the measurements of object centroids. New maximum-likelihood centroid positions were calculated from these modified frames and this experiment was repeated 1000 times for each of the objects. We find that it is highly improbable (with a chance of less than 1 in 1000) that the centroid shifts observed in objects 4-551, 4-141, 4-492 and 2-455 could be due to SNe offset from their host galaxy centers, as the brightnesses of these hypothetical events, constrained by the small observed brightness variations between epochs, are too small to affect the image profiles to the required extent. However, we find that there is a 5% chance that the apparent motion of object 2-766 can be explained by the SN hypothesis.

Thus, with the caveat that there are no pathological frame distortions on the scale of 1 to 2 arcsec, we are forced to conclude that object 4-551 shows significant PM, so it must be a nearby moving source, and that object 2-766 likely has measurable PM, though there is a small chance that the measured offset is an artefact of a SN superimposed on a galaxy. The faintest three candidates are low signal-to-noise photometric detections in the second epoch frames, so their PM measurements are more likely to suffer from unknown systematic errors. With these further caveats, it appears that object 4-492 has appreciable PM, while objects 4-141 and 2-455 have significant motion using what we consider to be the most sensitive procedure. For these sources, the detected PMs are much too low for Solar System objects, and since the two epochs were at almost identical times of the year, parallax is also ruled out. The only plausible alternative is that at least some of this sample of five objects are Galactic stars. This conclusion is supported by Méndez & Minniti (1999), who find that faint blue point sources are approximately twice as numerous in the HDF South than in the HDF (the HDF-S is located  $56^\circ$  from the galactic center, as opposed to  $110^\circ$  for the HDF).

## 6. FAINT, MOVING STARS?

What type of star could these sources be? If they were Galactic disk or thick disk stars they would have to be intrinsically faint in order to be seen at  $V \sim 28$ , since any intrinsically bright stars would be several tens of kiloparsecs out of the plane of the disk, and therefore not disk members. Indeed, stars with vertical heights of  $z < 10$  kpc above the plane of the Galaxy must have absolute magnitudes  $M_V > 12.6$  to be observed at  $V = 28$ . All known main-sequence populations are extremely red in  $V - I$  at these magnitudes. Disk white dwarfs (WDs) at the observed  $V - I$  colors would be about 1 Gyr old and have  $M_V$  near 13. This would again place them at about 10 kpc above the plane. However, our Galactic structure model (Ibata 1995) predicts an absence of disk, thick disk (both including WDs), or local spheroid stars blueward of  $V - I = 1.0$  at  $V \sim 28$ . Luminous spheroid stars at distances of  $\sim 100$  kpc may be found in the color-magnitude range  $27 < V < 29$ ,  $V - I < 1.0$ , but our Galaxy model predicts only 0.01 such stars in the HDF (though we caution the reader that no model has been properly tested in this regime). However, due to their enormous distances, the PMs of such stars would not have been detectable in our experiment. The observed moving stars therefore cannot belong to known disk, thick disk or spheroid popula-

tions.

## 7. ANCIENT WHITE DWARFS OF THE GALACTIC HALO?

No halo WDs were detected in the most sensitive survey to date (Knox *et al.* 1999), though it is possible that their detection limit was not as faint as claimed. So can the moving objects we have detected be halo WDs nevertheless? That the halo may contain numerous such stars has been suggested naturally (Kawaler 1996; Chabrier 1999) through the microlensing experiments which yield MACHO masses (Alcock *et al.* 1997) of  $0.5^{+0.3}_{-0.2} M_\odot$ , a value similar to the mass of  $0.51 \pm 0.03 M_\odot$  inferred for old WDs in ancient star clusters (Richer *et al.* 1997).

Until recently, cooling models of old WDs predicted that these stars should be quite red. However, new theoretical work (Hansen 1998, 1999; Saumon & Jacobson 1999), which extends the effective temperatures of WDs to below 4000 K, indicates that  $H_2$  provides strong opacity in the infrared, forcing the radiation out in the blue. Very old WDs, of age 12 Gyr, and mass  $0.5 M_\odot$ , have  $V - I \sim 0.2$  according to these models.

If the entire dark matter halo of the Milky Way were to be made up of such WDs there should be approximately 9 such objects in the HDF between  $27 < V < 28.5$ , they should have colors  $-0.2 < V - I < 1.0$ , and they should be situated at a mean distance of 1.2 kpc. Assuming an intrinsic one-dimensional velocity dispersion of  $200 \text{ km s}^{-1}$  for the dark halo population in the Solar Neighborhood, with zero net rotation about the Galactic center, the expected PM distributions (after correction for the Solar Reflex Motion) in both  $\mu_\ell$  and  $\mu_b$ , have a mean of  $-20 \text{ mas/yr}$  and a dispersion of  $35 \text{ mas/yr}$ .

The sample of moving objects we have discovered fits reasonably well into this model: correcting for the  $42\% \pm 2\%$  completeness of the HDF dataset between  $27 < I < 28$ , a total of about 4 stars are expected; their colors and magnitudes also agree with this model; and their PMs are consistent (at the 20% level) with being drawn from the expected distributions. Two of them (4-551 and 4-492) also appear to have spectral energy distributions consistent (within the large photometric uncertainties) with them being old WDs (see Table 1).

This suggests that we may have discovered, through their apparent PMs, a population of ancient WDs that are the local counterparts of the MACHOs. If this conclusion is correct, a substantial fraction of the dark matter concentrated in the inner regions of galactic halos would be baryonic and locked up in the form of very faint, blue (and therefore, ancient) WD stars. Further work is required to ascertain whether the problems of this scenario can be overcome, notably the requirement that stars form in a very restrictive mass range in the early Universe (Tamanaha *et al.* 1990), that the precursors of the WDs would make young galaxies appear anomalously bright (Charlot & Silk 1995), and that the interstellar medium would become over-enriched with heavy elements due to the material ejected from the WD progenitors (Gibson & Mould 1997).

By regarding our PM measurements as predictions, a direct test will be possible with third epoch observations of the HDF, to be obtained in December 1999 with the HST. Ultimately, however, spectroscopic observations will be needed to show whether or not these objects are WDs;

this may be feasible if nearer members of this population can be discovered.

The research of HBR and DS is supported in part by

the Natural Sciences and Engineering Research Council of Canada. RLG is supported under grant GO-6473.01-95A from STScI.

#### REFERENCES

- Alcock, C. *et al.*, 1997, ApJ 486, 697-726  
 Bergeron, P., Saumon, D. & Wesemael, F., 1995, ApJ 443, 764-779  
 Chabrier, G., 1999, ApJ 513, 103-106  
 Charlot, S. & Silk, J., 1995, ApJ 445, 124-128  
 Elson, R., Santiago, B., & Gilmore, G., 1996, New Astron., 1, 1-16  
 Flynn, C., Gould, A. & Bahcall, J., 1996, ApJ 466, L55-58  
 Gibson, B. & Mould, J., 1997, ApJ 482, 98-103  
 Gilliland, R.L., Nugent, P.E. & Phillips, M.M., 1999, astro-ph/9903229, ApJ, in press  
 Griest, K., 1991, ApJ 366, 412-421  
 Hansen, B., 1998, *Nature* **394**, 860-862  
 Hansen, B., 1999, ApJ 520, 680  
 Ibata, R., 1995, PhD Thesis, Cambridge  
 Ibata, R. & Lewis, G., 1998, AJ 116, 2569  
 Kawaler, S., 1996, ApJ 467, L61-64  
 Knox, R., Hawkins, M., Hambly, N., 1999, MNRAS 306, 736  
 Méndez, R., Minniti, D., de Marchi, G., Baker, A. & Couch W., 1996, MNRAS 283, 666-672  
 Méndez, R., Minniti, D., 1999, ApJL submitted  
 Richer *et al.*, 1997, ApJ 484, 741-760  
 Saumon, D. & Jacobson, S., 1999, ApJ 511, L107-110  
 Stetson, P., 1987, PASP 99, 191-222  
 Tamanaha, C., Silk, J., Wood, M., Winget, D., 1990, ApJ 358, 164-169  
 Thompson, R.I., Storrie-Lombardi, L.J., Weymann, R.J., Rieke, M.J., Schneider, G., Stobie, E. & Lytle, D., 1999, AJ 117, 17-39  
 Trauger, J., Vaughan, A., Evans, R., Moody, D., 1995, edited by A. Koratkar and C. Leitherer (STScI, Baltimore), pp. 379-385  
 Williams, R. *et al.*, 1996, AJ 112, 1335-1389 (W95)

TABLE 1  
 FAINT STARS WITH DETECTED PROPER MOTION.

| ID    | I     | V-I  | B-V   | U-B   | V-J   | $\mu_\ell, \mu_b$     | $d$      | $v$      | Method 1                         | Method 2                         | Method 3                         | Method 4                         |
|-------|-------|------|-------|-------|-------|-----------------------|----------|----------|----------------------------------|----------------------------------|----------------------------------|----------------------------------|
|       |       |      |       |       |       | (mas/yr)              | (kpc)    | (km/s)   | $\delta x, \delta y$<br>(mas/yr) | $\delta x, \delta y$<br>(mas/yr) | $\delta x, \delta y$<br>(mas/yr) | $\delta x, \delta y$<br>(mas/yr) |
| 4-551 | 27.54 | 0.40 | >1.76 | ...   | -0.98 | 15.1(4.5), -17.4(5.0) | 1.3(0.1) | 220(60)  | -21(5), 9(5)                     | -14(9), 5(9)                     | -19(2), 4(2)                     | -20(9), 8(9)                     |
| 2-766 | 27.66 | 0.83 | 0.18  | -0.09 | ...   | -17.6(4.9), 19.0(5.1) | 1.7(0.3) | 280(100) | -24(5), 11(5)                    | -21(9), 1(9)                     | -15(5), 4(4)                     | -21(9), 3(9)                     |
| 4-141 | 28.05 | 0.04 | -0.24 | 0.47  | ...   | 29.4(5.3), 18.2(6.0)  | 1.4(0.2) | 400(80)  | 9(6), 34(5)                      | -1(9), 16(9)                     | 3(5), 9(4)                       | 5(9), 18(9)                      |
| 4-492 | 28.57 | 0.45 | >1.07 | ...   | -0.17 | -2.9(6.5), 18.1(5.6)  | 2.2(0.4) | 320(120) | 18(6), 3(6)                      | 17(9), -6(9)                     | 20(5), 6(4)                      | 21(9), 8(9)                      |
| 2-455 | 28.65 | 0.17 | 0.37  | >0.00 | ...   | 42.5(7.4), -28.6(6.3) | 2.0(0.3) | 520(160) | 40(6), -32(8)                    | -13(9), -8(9)                    | 2(15), 4(11)                     | -1(9), -12(9)                    |
| model | ...   | 0.38 | 1.51  | 0.70  | -0.38 | ...                   | ...      | ...      | ...                              | ...                              | ...                              | ...                              |

NOTE.—Column (1) notes the W95 identification label, and columns (2) to (6) give the calibrated isophotal AB photometry from W95 and Thompson *et al.* (1999). Column (7) lists the PM results, where  $\mu_\ell$  and  $\mu_b$  are the PMs in the direction of, respectively, Galactic longitude and Galactic latitude. The last row in the table labelled ‘model’ contains the expected colors from a 0.5 M $_{\odot}$  hydrogen-rich white dwarf with an effective temperature of 3000 K (Hansen 1999). Columns (8) and (9) list, respectively, the distance and velocity (corrected for the Solar reflex motion) inferred from that white dwarf model. Columns (10) to (13) show the PM results from different measurement techniques. The  $\delta x, \delta y$  offsets listed are parallel to the CCD axes. Method 1 is the maximum-likelihood technique applied to individual frames. Method 2 is the positional difference in a Gaussian PSF model fit to the object profiles in the combined frames at each epoch. Method 3 is a two-dimensional cross-correlation of a small  $3'' \times 3''$  region of the combined images at the two epochs around each of the objects (with a  $1''$  cosine-bell tapering region applied to the edges). Finally, method 4 involves a Gaussian PSF fit to the object profiles, but this time using images combined with four-times oversampling in an independent analysis for a separate project (Gilliland *et al.* 1999). The uncertainties in methods 2 and 4 have been estimated by comparing two equal exposure subsets of the first epoch dataset, where there is no possibility of real motion. The uncertainty in method 3 is derived from a fit to the correlation function.

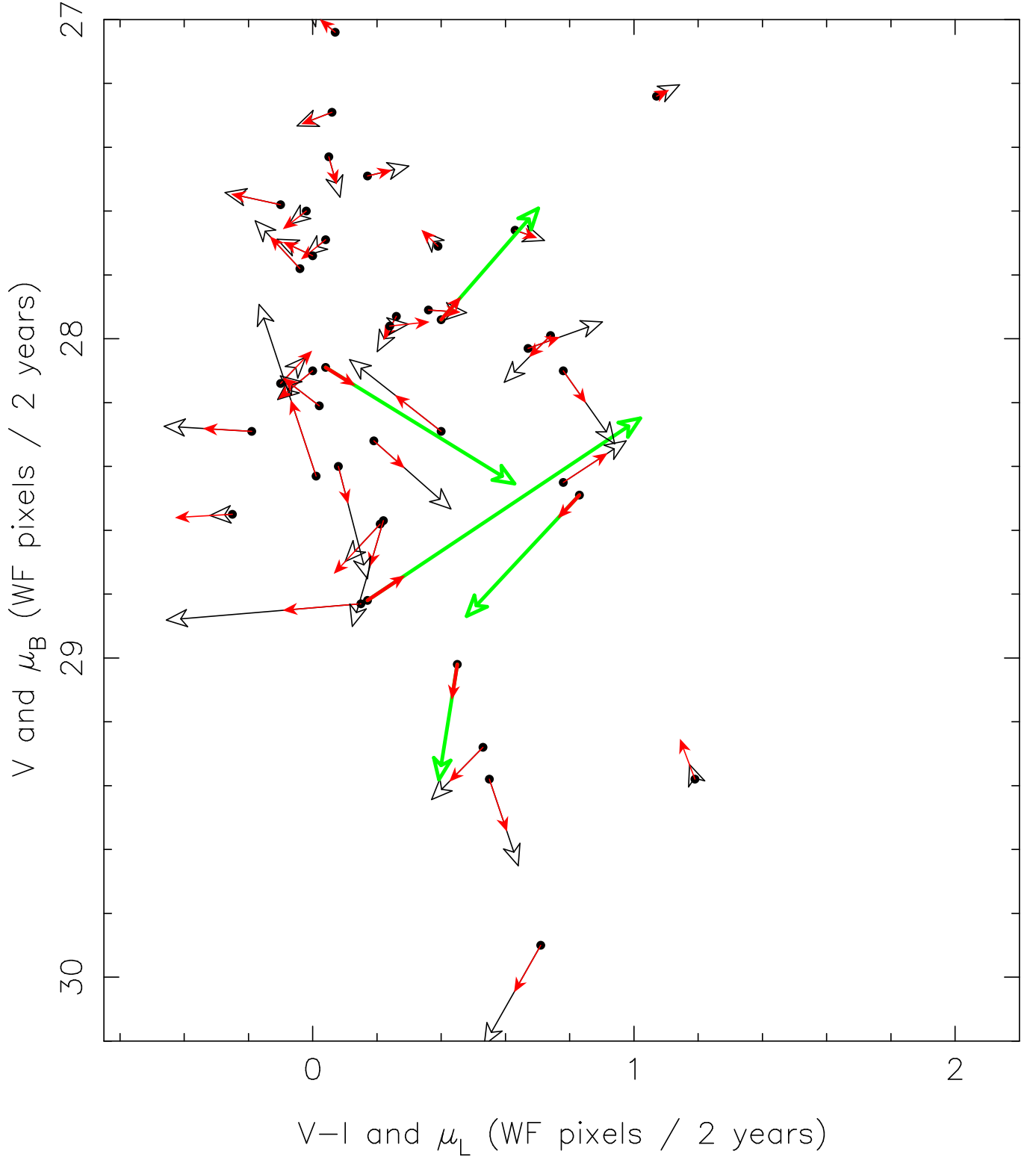


FIG. 1.— The faint end of the color-magnitude diagram of the HDF showing the 40 faint unresolved objects together with their PMs.

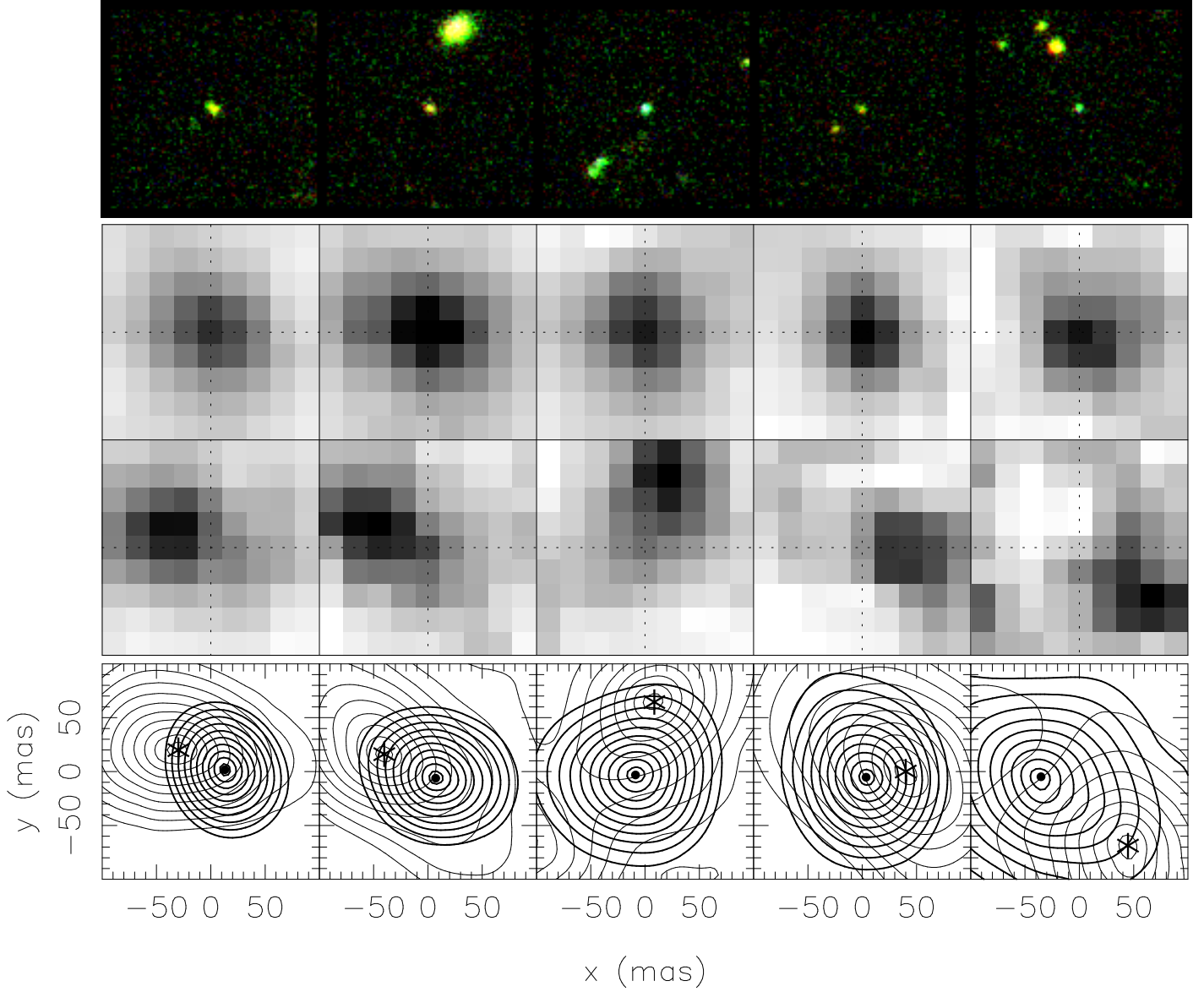


FIG. 2.— The five faint, apparently moving objects. The panels show, from left to right, images and likelihood contours of the five faint objects with significant PM: 4–551, 2–766, 4–141, 4–492 and 2–455. The color images in the top row show the immediate field ( $4'' \times 4''$ ) around each object; RGB intensities indicate, respectively, the fluxes in the F814W, F606W and F450W filters. High resolution images of these objects were constructed by using the PSF model to redistribute the flux from the individual WF frames onto a  $4\times$  oversampled grid (i.e.,  $0''.025/\text{pixel}$ ); these images, for the first and second epoch datasets are displayed, respectively, in the second and third rows. The same  $0''.2 \times 0''.2$  region of the sky is shown for each object, and cross-hairs have been added at the position corresponding to the centroid location in the first epoch image. The bottom row shows the corresponding likelihood contours of the object centroids obtained from the first epoch data (thick lines) and the second epoch data (thin lines). The contour intervals are such that the  $n$ th contour marks the boundary of the region where the likelihood has fallen by a factor of  $\exp -\frac{n^2}{2}$  from the most likely value.